WCTE 2020
WORLD CONFERENCE ON TIMBER ENGINEERING
SANTIAGO, CHILE | 24 - 27 AUGUST

PERPENDICULAR-TO-GRAIN COMPRESSION BEHAVIOUR OF SCREW REINFORCED TIMBER AND A NOVEL APPLICATION OF DIGITAL IMAGE CORRELATION

Joe Tompkins[1], Panayiotis Papastavrou[2], Simon Smith[3], Tristan Wallwork[4], Allan McRobie[5]

ABSTRACT: This project investigates various factors which influence the behaviour of a timber roof structure designed by Smith & Wallwork Engineers. The first part of the project focused on material of sweet chestnut, where Digital Image Correlation (DIC) was employed to obtain values for the shear modulus. DIC was able to implement the shear field test method prescribed in BS EN 408:2010, along with two new methods developed based on additional information available through DIC. These methods were accurate, fast to implement, and potentially more robust than the shear field test method. A method to estimate the true value of the Timoshenko shear coefficient was also developed. The second section of the project involved physical testing of portions of the roof structure to investigate the behaviour of screw-reinforced and unreinforced timber loaded perpendicular to grain. Together with finite element modelling, it was noticed that a key aspect of the connection's behaviour was the axial force transfer between overlapping screws via shear in the timber, and the resulting relative displacement between the screws. A simple spring model was developed to characterise the compression stiffness of the roof which can now be used in reverse to calculate the forces due to moisture expansion or contraction.

KEY WORDS: Screw reinforced timber, Perpendicular to grain stiffness, Digital Image Correlation, Material testing

1 INTRODUCTION

A research project was undertaken at the University of Cambridge into the behaviour of reinforced and unreinforced timber loaded perpendicular to grain. The project involved full-scale physical testing of joints and employed a novel application of Digital Image Correlation. Together with finite element modelling, these led to the development of a simple spring model to characterise the compression stiffness of a complex stacked timber roof.

2 MOTIVATION

2.1 THE ROOF STRUCTURE

The project was based on a roof structure designed by Smith and Wallwork Engineers in collaboration with Niall McLaughlin Architects. It is a complex two-way spanning ten-layered grid of 44mm x 150mm structural sweet chestnut timber members, with a pyramidal volume removed from the bottom to create a vaulted space below.

There are 4 bays of 4.8m x 4.8m each. The connection details are highly complex (see Figure 2), including small screw spacings, fully threaded screws and a staggered vertical layout. Furthermore, the entire structural depth of the roof is made up of timber loaded perpendicular to grain.

Figure 1: *Architectural model of single bay of roof structure*

Due to the perpendicular to grain stacking of the structure, a conservative analysis was carried out and allowed for high differential movement in the design of the roof structure between the stacked timber lattice and

[1] Joe Tompkins, Structure Workshop, London, UK, jt@structureworkshop.co.uk
[2] Panayiotis Papastavrou, Smith and Wallwork Engineers, Cambridge, UK, panayiotis@smithandwallwork.com
[3] Simon Smith, Smith and Wallwork Engineers, Cambridge, UK, simon.smith@smithandwallwork.com
[4] Tristan Wallwork, Smith and Wallwork Engineers, Cambridge, UK, tristan.wallwork@smithandwallwork.com
[5] Prof. Allan McRobie, Cambridge University Engineering Department, Cambridge, UK, fam@eng.cam.ac.uk

the perimeter interface details. The project aimed to further understand the movement behaviour by considering 3D load spread and screw reinforcing effects for the elastic and drying shrinkage related movement.

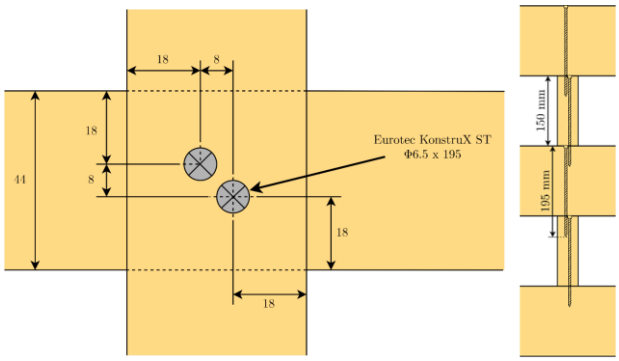

Figure 2: *Plan and elevation of connection detail from roof (lengths in mm)*

2.2 DIGITAL IMAGE CORRELATION FOR MATERIAL TESTING

The structural sweet chestnut for the roof was quoted as having structural properties equivalent to D30 to BS EN 338:2016 [1] by the specialist timber supplier Inwood, although this was thought to be conservative. Thus, before testing the specific joint geometry, the basic stiffness properties of the sweet chestnut were ascertained. However, standard testing procedures described by BS EN 408:2010 [2] require specialist equipment and large specimen sizes, so Digital Image Correlation (DIC) was investigated, since the only equipment required is a loading frame, a high-resolution camera and a suitable computer programme, and the specimens can be sufficiently small to allow the use of a typical dual-column tabletop Universal Testing Machine.

3 MATERIAL TESTING

The first section of the project focused on the testing of the three material properties of sweet chestnut deemed to be the most pertinent to the roof's deflection behaviour: the modulus of elasticity in bending, $E_{m,g}$, the modulus of elasticity perpendicular to grain in compression, $E_{c,90,}$ and the shear modulus, G.

3.1 EXPERIMENTAL DESIGN

Testing was carried out in accordance with BS EN 408:2010 as closely as possible, although some requirements regarding instrumental accuracy and environmental conditions were not achievable given the equipment available.

The experimental process involved testing of two batches of sweet chestnut samples. The first batch were long, thin samples used in a four-point-bend test to find both the modulus of elasticity in bending and the shear modulus, while the second batch were cuboid samples tested in simple compression to find the compression modulus perpendicular to grain.

All material testing was carried out using a dual-column 10kN Instron Universal Testing Machine, and thus the length of the long samples was defined by BS EN 408:2010, as were all the dimensions of the block samples. All samples were "clear", i.e. free of knots/wane with grain closely aligned with the sample dimensions, and were provided by Inwood timber.

Figure 3: *Experimental set up of material tests*

3.2 INTRODUCTION TO DIC

Digital Image Correlation is a measurement and visualisation technique which allows the computation of quasi-continuous 2D displacement and strain fields on the surface of a test sample.

To compute these values, the sample surface is prepared using spray paint to generate a random pattern of fine speckles, and the surface is photographed in the unloaded and loaded state. Processing software then divides the unloaded photograph into individual squares ("subsets") and performs a normalised cross-correlation with the loaded photograph to find the new position of these subsets, initially giving pixel-accurate values of displacement. This is improved by fitting a polynomial to the peak of the correlation function, giving sub-pixel accuracy.

Once sub-pixel accurate values are found, the displacement field is smoothed to remove some of the noise in the signal. This step is particularly important, since, unlike traditional strain gauges which measure strain directly, DIC measures displacement and differentiates to find the strain field, and thus any high-frequency noise that remains after smoothing is magnified (see Section 3.3.5).

For this project, a MATLAB code written by Allan McRobie [3] was used.

3.3 SHEAR MODULUS

Instead of the equipment suggested for the shear field test method in BS EN 408:2010, DIC was used to measure the shear modulus. This proved to be an effective application of the technology: DIC was able to implement both the prescribed method and two new methods which were developed based on the additional information available through the use of DIC.

3.3.1 Prescribed Method

The method prescribed in section 11.2 of BS EN 408:2010, the 'Shear Field test method' involves the measurement of changes in the length of the diagonals of a square marked onto the side of the sample, then calculating the shear strain using the average of the two diagonal deformations to eliminate the influence of flexural deformation. The calculation includes a

correction factor, α, to account for the non-uniform shear stress distribution, based on the size of the square considered:

$$\alpha = \frac{3}{2} - \frac{h_0^2}{4h^2} \quad (1)$$

Where h_0 is the initial length of the diagonal of the square, such that, when the square is the same depth as the sample, α = 1. The use of DIC allowed extra flexibility in the implementation of this method since the size of the measurement region is defined in post-processing rather than fixed by the size of the measuring equipment. Thus, two square sizes were used to check whether this correction is appropriate.
The results obtained from this method were slightly higher than the D30 value for G_{mean}, with relatively consistent results for each sample.

3.3.2 Alternative Methods

To explore the potential of DIC as a material testing method, two novel methods were also carried out which make use of the shear strain distribution, both of which were based on Timoshenko beam theory. The first method involves calculating the average neutral axis strain in the region of constant shear stress, then converting to G_{mean} using two different values of the Timoshenko shear coefficient, K, which is defined by Equation (2):

$$\int_A \tau \, dA = KGA\gamma_{NA} \quad (2)$$

The two values chosen were K = 2/3 and K = 5/6, as these are the most commonly used values for rectangular sections (most empirical rules, such as those given in Kaneko, T., 1975 [4], give values between these two).
Given the difficulty of defining an accurate value for the Timoshenko shear coefficient [4], the second method attempts to avoid defining a value altogether. To do this, the shear strain distribution was integrated over the cross-section, and the shear modulus found using the following equation:

$$V = \int_A \tau \, dA = G \int_A \gamma \, dA$$

$$\therefore \; G = V \Big/ \int_A \gamma \, dA \quad (3)$$

For both methods, the shear strain distribution was assumed to be constant through the cross section. This could be verified by using a second camera to photograph the opposite side of the sample, although this was not available.
Both novel methods gave good agreement with the prescribed method and were simple and fast to implement. Since they incorporated a larger amount of information, it is possible that these methods are more robust than the suggested 'Shear Field test method'.

3.3.3 Results

The results from the various analysis methods gave good alignment. Table 1 shows a summary of the values obtained:

Table 1: *Shear modulus results from DIC*

Method		G_{mean} [MPa]	Std. Dev. [MPa]
BS EN 408:2010	L=10h/11	868	219
	L=8h/11	905	212
Neutral Axis	K=2/3	974	224
Strain	K=5/6	780	179
Strain Integral		876	242

The two values obtained using different square sizes are relatively similar and correspond to a shear coefficient value of approximately K = 0.73. All these values are greater than the shear modulus given for strength class D30 of 690 MPa.
The standard deviation from each method was high, although this arose due to the variability in the timber rather than the lack of precision in the analysis methods – values for each individual sample were relatively consistent between methods. A greater sample size should be used to obtain more reliable values of the material properties.

3.3.4 Method to estimate Timoshenko coefficient, K

It should be noted that the correction factor, α, in the BS EN 408:2010 method implicitly assumes a shear coefficient of K = 2/3. Since the two values of G obtained using this value of K are different, with the value based on a smaller square being the larger of the two, this indicates the true value of K is in fact greater than 2/3.
An estimate of the true value of K was found by iterating between the BS EN 408 method and the neutral axis strain method: first, an equivalent value of K was found at each iteration by inserting the average of the values of G for different size squares into Equation (2). The correction factor, α, was then redefined as:

$$\alpha = \frac{1}{K} - \left(\frac{1}{K} - 1\right)\frac{h_0^2}{2h^2} \quad (4)$$

such that at $h_0 = 0$, $\alpha = 1/K$, and at $h_0 = \sqrt{2}$, $\alpha = 1$. Thus, a new pair of values of G were found using the BS EN 408:2010 method. The two values converge until a self-consistent pair of values of G was found of G_{mean} = 840 MPa, which corresponds to a shear coefficient of K = 0.764. As expected, this lies between K = 2/3 and K = 5/6.
This iterative process could easily be integrated into an automated algorithm to improve the accuracy of the method suggested by BS EN 408:2010.

3.3.5 Smoothing Algorithms

The MATLAB code used for DIC originally employed a Savitsky-Golay filter: a widely used smoothing algorithm which functions by locally fitting a polynomial to a sliding window of data [5]. The level of

smoothing is defined by two main factors: the size of the window, and the order of polynomial. A larger window will ignore smaller variations in strain, as will a low-order polynomial.

This algorithm is particularly effective for use in DIC, since it provides a low computation effort method for calculating the strain field from the smoothed displacement field: each data point is the origin of its own locally fitted polynomial, so the derivatives of these fitted polynomials (i.e. the strains) are simply the coefficients of the first-order terms.

Initially, a third-order polynomial was used with a filter window of 5x5 subset squares, followed by a 9x9 window, but these did not achieve sufficient smoothing. Figure 4 shows the signal noise drowning the shear strain distribution.

Since the loading arrangement in material testing is controlled, the geometry of the samples is regular and the samples are free of knots, it can be assumed that the true strain distribution is simple, and is free of high-frequency components. This means that the degree of smoothing can be greatly increased.

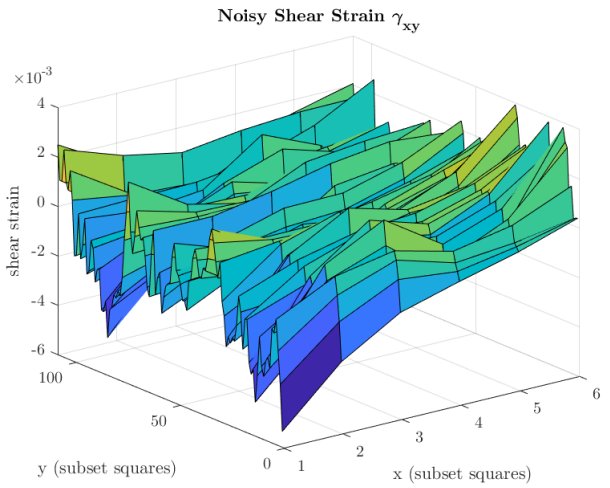

Figure 4: *Shear strain with 5x5 Savitsky-Golay filter*

The logical extension of the Savitzky-Golay filter was to extend the window to include the entire data field, thus replacing the displacement data with a polynomial approximation of the whole distribution. Since the larger variations in the displacement distributions were very smooth, second-order polynomials were sufficient to give an excellent fit. Figure 5 shows an entirely smooth strain distribution produced following this method, from which values of the shear modulus were calculated.

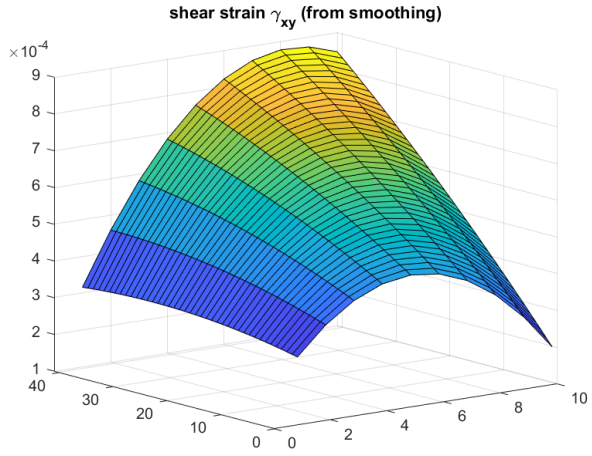

Figure 5: *Shear strain from fully smoothed displacement field*

3.3.6 Advantages and Disadvantages of DIC

There are clearly advantages and disadvantages of DIC when compared to the use of strain gauges for material testing, in particular for obtaining the shear modulus. The advantages include:

- DIC allows use of smaller samples since it is not limited by size of displacement transducers.
- Can use alternative methods which account for the whole strain field rather than discrete points, so less susceptible to incorrect data points.
- Material testing only requires a macro picture of the strain field to obtain material properties so a consumer-grade camera is suitable, and thus lower cost in comparison to high-spec cameras needed for measurement of smaller strain variations.
- DIC allows additional flexibility in the application of the BS EN 408 method, as control points do not need to be pre-defined.

The disadvantages include:

- Even consumer-grade digital cameras are expensive in comparison to strain gauges.
- Difficult to apply spray paint to provide a good distribution of fleck size and randomness.
- Without automated post-processing, the overall process takes longer than analogue methods.

Overall, it seems that the advantages of DIC could potentially justify the additional expenditure versus strain gauges, and several testing laboratories may already have access to all the required equipment. Automated post-processing would likely make the process faster than analogue methods. Thus, for larger material testing laboratories, DIC seems to be a highly promising technology.

3.4 BENDING MODULUS AND PERPENDICULAR TO GRAIN MODULUS

The bending modulus, $E_{m,g}$, was obtained in the same four-point-bend test as the shear modulus, but the value was found via measuring the central deflection using a C-clip transducer. Using equations given in BS EN 408, the bending modulus was found using a portion of the

load-deflection graph which gave sufficiently good alignment to a straight line. Two values were found, one of which includes a correction for the central deflection due to the low shear stiffness of timber.
The mean uncorrected value was 11.66 GPa, while the mean corrected value was 12.12 GPa, with standard deviations of 0.996 GPa and 1.076 GPa respectively. These both compare favourably to the mean value of 11 GPa for strength class D30.
The compression modulus perpendicular to grain, $E_{c,90}$, was found in a simple compression test by measuring the change in a gauge length using a laser transducer. The mean value of $E_{c,90}$ was 674 MPa, with a standard deviation of 119 MPa. This is less than the D30 value of 730 MPa. Table 2 gives a summary of these results.

Table 2: *Material testing results*

Property	Mean [MPa]	Std. Dev. [MPa]
$E_{m,g}$ (uncorrected)	11660	996
$E_{m,g}$ (corrected)	12120	1076
$E_{c,90}$	674	119
G_{mean}	See Table 1	

4 ROOF STRUCTURE MODELLING

The second part of the project aimed to understand the compression behaviour of the roof structure in more detail. Prior to the tests, Smith & Wallwork had modelled the compression behaviour of the roof as a series of square timber columns, 44 mm x 44 mm on plan, 150mm high, at each timber-to-timber contact point. However, this neglected the spreading of the load through the depth of the timber beams, and the reinforcing effect of screws under perpendicular to grain compression.
To investigate these aspects of the design, physical testing and finite element modelling were carried out on a cut-out portion of the roof structure. This was effectively a stack of timber members tested in simple compression, and two stacks were tested to discriminate between the two effects of load spreading and screw reinforcement: one without screws and one with screws as per the connection design in Figure 2. For the physical tests, the stack was tested at 1:1 scale using sweet chestnut provided by Inwood, such that the compression stiffness would accurately emulate that of the real roof. For the finite element models, 3D-continuum mechanics models were built using Abaqus [6], with values of stiffness taken from the material testing carried out in the first section. For the screwed stack, the screws were modelled with tie constraints along the full length of the shanks since the screws are fully threaded.
Figure 6 shows the finite element model of the screwless stack built in Abaqus, while Figure 7 shows a stack in the test rig.

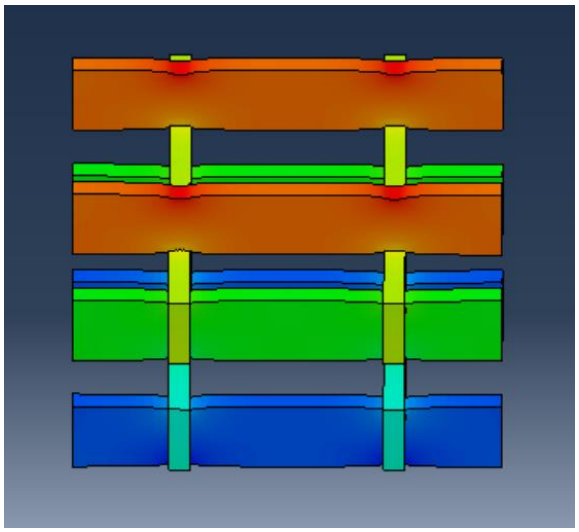

Figure 6: *Deformed finite element model of screwless stack (mesh not shown). Deformation greatly magnified.*

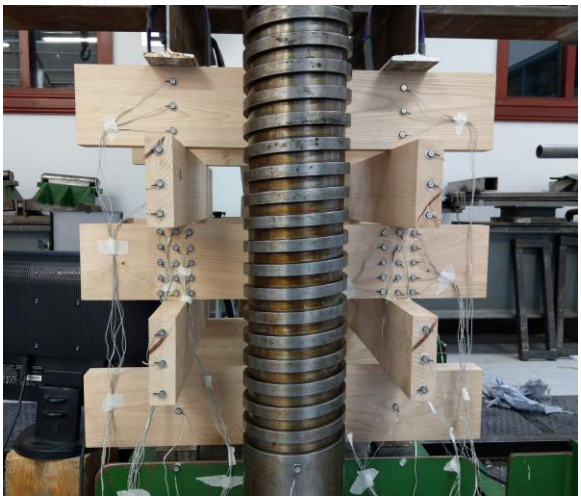

Figure 7: *Portion of roof structure in testing rig*

4.1 FINITE ELEMENT MODELLING

The finite element models served several purposes: prior to physical testing, they gave initial stiffness estimates; after testing they assisted in verifying the validity of the observed load paths; and most importantly, they provided invaluable insights into the internal load paths of the screwed stack, leading to the development of the simple spring model (see Section 4.3).

4.2 PHYSICAL TESTING

4.2.1 Experimental Design

The experiment was carried out in a large Amsler testing machine which measured both the deflection of the loading platen and the load in the stack. Several other methods of measurements were also used, including horizontal transducers to monitor the possibility of buckling, and DIC which was used following the tests to visualise the stress paths.

4.2.2 Results

Figure 8 shows the load versus displacement graphs for the two stacks. During both tests, there was an early loss of stiffness due to improper tightening of the upper

platen. Once this slack was taken up, both stacks began to displace in a linear manner.

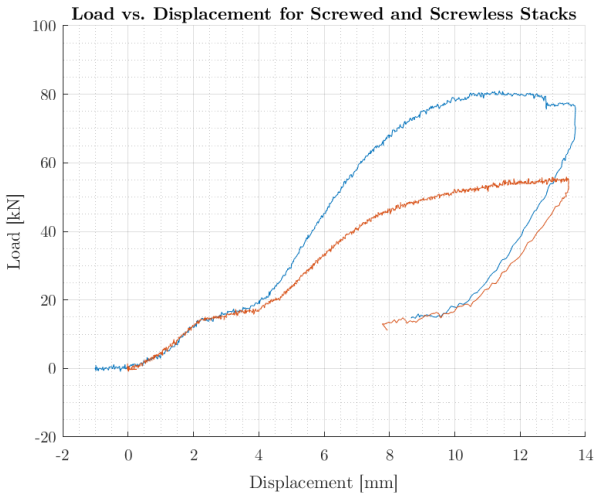

Figure 8: *Load vs displacement curves for both stacks. Orange: screwless stack; blue: screwed stack. N.b. the origin of the screwed stack curve has been adjusted for clarity such that the initiations of the early loss of stiffness coincide.*

From Figure 8, it can be seen that both stacks suffered a gradual loss of stiffness at high loads before unloading elastically. This was due to the development of a buckling mode, and so the tests were halted before catastrophic failure occurred.

To establish the stiffness of each of the stacks, a linear model was fitted to the linear portion of each curve after the loss of stiffness. The gradient of these models provided an "equivalent member stiffness", $(EA/L)_e$, for the stacks as a whole. The stiffnesses found were **$(EA/L)_e$ = 9.219 kN/mm** for the screwless stack and **$(EA/L)_e$ = 14.41 kN/mm** for the screwed stack.

These stiffnesses were both less stiff than their counterpart Abaqus models, both by a factor of approximately of 0.6. Following comparisons of the load paths observed by DIC and the measured nodal displacement in the physical testing against the Abaqus models, it was decided that it would be appropriate to use the Abaqus model to obtain values of internal displacements for further modelling, but these values were then scaled to match the experimental overall stiffness (see Section 4.3).

4.2.3 Discussion: Screwless Stack

To evaluate the increase in stiffness of the screwless stack due to the spreading of load, the "equivalent member stiffness" of the 44 mm x 44 mm square timber columns was calculated. Using $E_{c,90}$ = 670 MPa as per the material tests, the stiffness was found as EA/L = 6.918 kN/mm. Thus, the spreading of the load path provided an increase in stiffness of 33.3%.

Table 3: *Equivalent stiffnesses of models/samples*

Model	Equiv. Stiffness [kN/mm]
Simple timber columns	6.918
Screwless stack	9.219
Screwed stack	14.41

This load path was then visualised using DIC. Figure 9 shows the vertical strain and shear strain on the side of the middle layer of the stack. The spreading of load through the depth of the beam can clearly be seen, as can the reduction in stress. Figure 10 shows the same strain pattern visualised in the Abaqus model of the screwless stack, showing very strong alignment.

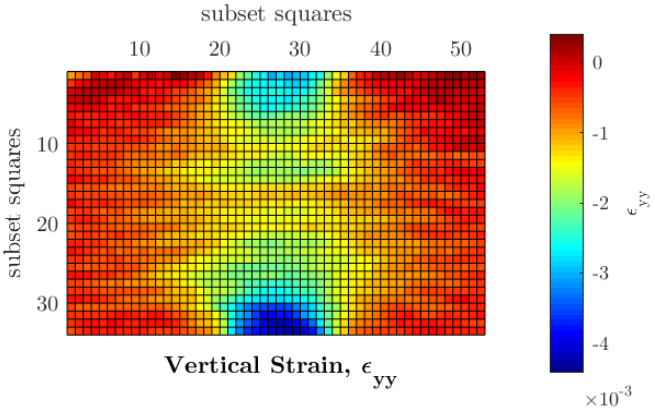

Figure 9: *Vertical strain distribution as measured by DIC*

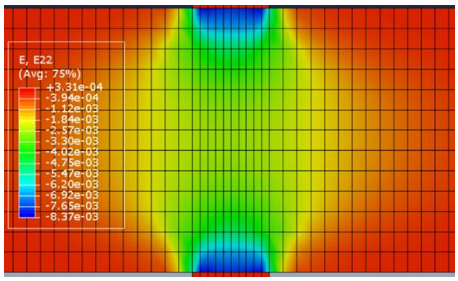

Figure 10: *Vertical strain distribution from Abaqus model (n.b. scales are not comparable due to different load intervals)*

4.2.4 Discussion: Screwed Stack

Prior to the testing process, the influence of the screws on the 'member stiffness' of the roof was unknown and unaccounted for. An initial simple estimate of the stiffness was obtained by modelling the screws as a single, long screw inserted into the screwless stack which develops fully composite action. The stiffness of a long screw was $(EA/L)_{e,screw}$ = 17.81 kN/mm, which, when taken in "parallel" with the screwless stack, gives a composite stiffness of $(EA/L)_{e,composite}$ = 27.03 kN/mm - an increase of 193% versus the screwless stack.

In reality, the screwed stack stiffness was only just over half this stiff, or alternatively are developing a 'degree of composite action' of (14.41 - 9.219)/17.81 = 0.291. Furthermore, the stiffness of the screwed stack is in fact less than the estimate for a single screw, $(EA/L)_{e,screw}$.

Based on interrogation of the Abaqus model, it became clear that this reduction in stiffness arose from the nature of the connection, specifically the region of overlap between the screws, and the transfer of axial load between them through shear in the timber 'matrix'. This effect is explored further in Section 4.3.

Relative to the stiffness of the simple timber columns, the screwed stack gave an increase in stiffness of 108%, a value which was integrated into Smith and Wallwork's design.

4.2.5 Buildability

Testing the stacks at 1:1 scale offered an early opportunity to prototype the roof structure and test the buildability. This was of concern as there were several factors which made the connection difficult to fabricate. Firstly, the small screw spacings and edge distances combined with the stacking nature of the structure mean the fabrication tolerances are extremely tight. Secondly, the slenderness of the screws/drill bits made them prone to diversion while cutting through the timber. Finally, since the holes were relatively deep, the verticality of the drill bit and sample were of great importance.

Initial attempts to drill these holes were unsuccessful, so a complex method was developed which required three holes to be drilled per screw. While this produced good results, it would present a serious programme problem for the real roof structure which contains almost 5000 screws.

After relaying these insights from the prototyping process to the design team, the design for the roof was amended to use fewer screws in the more lightly loaded regions of the structure.

4.3 SPRING MODEL

Through the Abaqus model, it was noticed that a key aspect of the connection's behaviour was the axial force transfer between overlapping screws via shear in the timber. Figure 11 shows the shear stress perpendicular to grain as modelled in Abaqus.

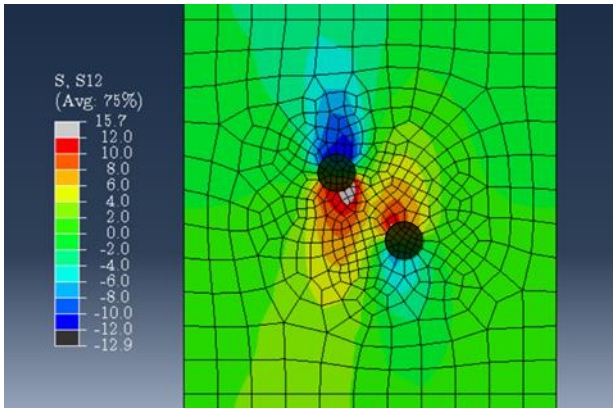

Figure 11: *Shear stress perpendicular to grain in region of axial force transfer between screws.*

To visualise the effect of this phenomenon, the displacement of each end of the screws was taken from the Abaqus model at the working load of 44kN and plotted against their depth from the top surface of the stack. This is shown in Figure 12.

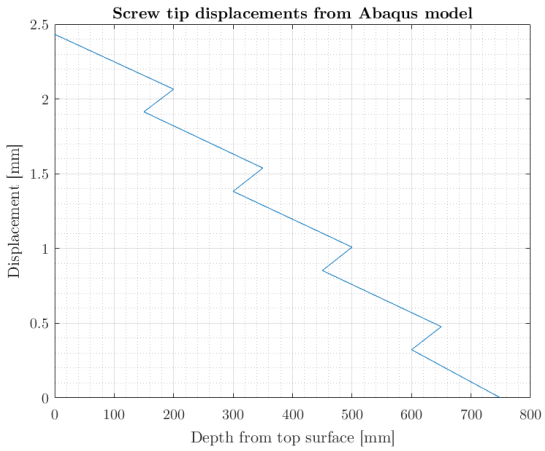

Figure 12: *Screw tip displacements versus position in stack*

By plotting the spacing of the screw tips to scale as in Figure 12, this phenomenon can be seen clearly: the sections of negative gradient represent the stiffness of the screws and the timber acting in composite with them, while the "backward steps" of positive gradient show the relative displacement between the tips of adjacent screws due to axial force transfer. This can be verified by checking the stiffnesses: taking the gradient of one 'screw', the equivalent stiffness is 24.6 kN/mm, which is far closer to the predicted value of 27.03 kN/mm.

4.3.1 Development of Spring Model

A one-dimensional spring model was built to attempt to capture this phenomenon of rolling shear deflection between overlapping screws. To develop the model, the screws were directly modelled as springs, then a "shear spring" was added between the bottom of one "screw" and the top of the next. A final spring was added to represent the timber in the regions of no screw overlap. Figure 13 shows the complete model. The model is defined by three spring constants, EA_s, EA_G and EA_t whose values were initially chosen based on simple estimates.

EA_s was modelled on the 4.5mm shank diameter, while EA_t was based on the 44 mm x 44 mm columns originally modelled by Smith and Wallwork. To choose a value for EA_G, the loaded area between the screws was modelled using a 'throat area' under shear between the two screw shafts equal to the distance between their centres (12mm). A shear modulus of 870 MPa was used. Since the shear zone is modelled as a linear spring of 50 mm length rather than a shear zone of 12 mm length, the spring constant was scaled accordingly. All spring constants were also scaled by a factor of 4 to account for the 4 corners of the stack. Table 4 gives the initial estimates of the spring constants.

Table 4: *Spring constant initial values*

Spring constant	Value [N]
EA_s	13.4×10^6
EA_t	5.19×10^6
EA_G	8.70×10^6

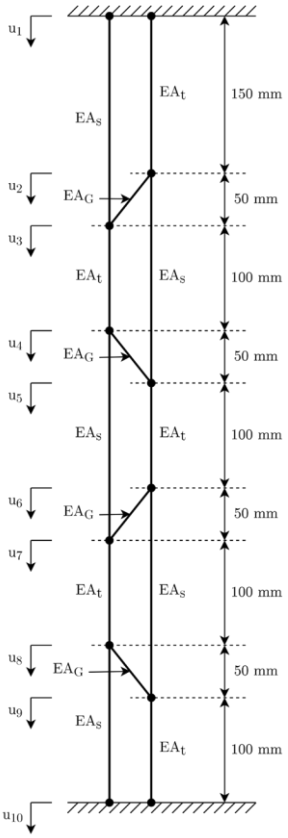

Figure 13: *Spring model of screwed stack.*

To obtain results for the spring model, a force of 44 kN was applied to the top node (node 1), and a zero-deflection boundary condition was applied to node 10, where 44 kN was the estimated working load for the actual roof design. The results are plotted in Figure 14 alongside the scaled values from the Abaqus model. They give the approximate correct shape, showing the "backward step" pattern, but the model is too stiff overall.

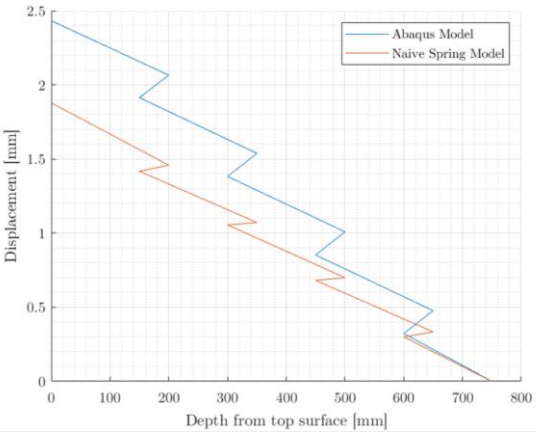

Figure 14: *Results of initial spring model versus Abaqus model*

4.3.2 Optimisation of Spring Model

To improve the accuracy of the spring model, modification factors were applied to each of the spring constants, such that the spring constants became M_sEA_s, M_tEA_t and M_GEA_G. A script was written to iterate through various combinations of these modification factors, recalculate the stiffness matrix and nodal displacements, and find the set of values with the lowest residual sum of squares (RSS) value versus the Abaqus model.

The optimised model gave an extremely good fit to the Abaqus values. Figure 15 shows the spring model plotted alongside the Abaqus model.

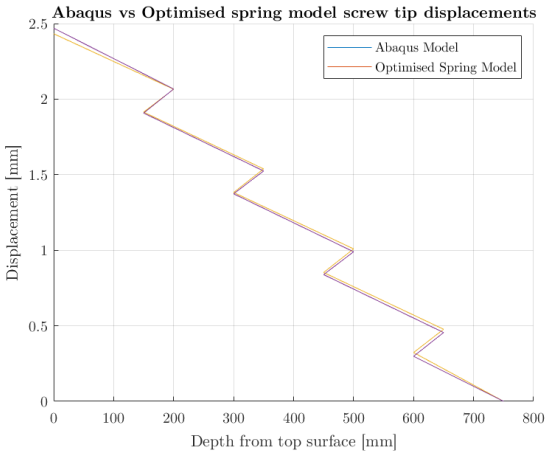

Figure 15: *Optimised spring model versus Abaqus model*

Table 5: *Optimised modification factor values*

Modification factor	Value
M_s	1.55
M_t	0.12
M_G	1.348

Table 5 gives the final values of the modification factors. While the resolution of the spring model is not great enough for these factors to align exactly with physical phenomena, some insights can still be gained. For example, M_s is greater than 1, which represents the stiffness of the timber acting in composite with the screws. M_t is less than 1, since much of the timber stiffness has been absorbed into the "screw spring", and as such this spring potentially represents the timber not acting compositely with the screw.

The value of M_G is influenced by several factors: firstly, the axial force transfer between screws occurs via shear both perpendicular and parallel to grain, since the layout of the screws is not aligned with the grain direction. This means that the 'effective' shear modulus will be some value between the shear modulus and rolling shear modulus. This effect alone would lead to a value of M_G less than 1, but in fact the value of M_G was greater than 1. This is potentially due to the compression stiffness of the timber in the overlap region, or potentially due to the 'throat area' model not being accurate. An improvement to this model could account for the timber surrounding the screws on all sides, since Figure 11 shows significant shear stress in the regions on the opposite sides of the screws.

With the highly optimised spring constants, the spring model can now be used by Smith and Wallwork to predict deflections of the roof structure under compression, and can also be used in reverse to predict the forces induced by moisture expansion or contraction.

This is a primary design consideration for the structure since the full structural depth is built up from perpendicular-to-grain timber members. Whilst no attempt has been made to restrain this expansion/contraction in the design via the screw connections, this may prove to be possible via use of this tool to predict this behaviour, which would lead to lower long-term settlement than allowed for.

5 POTENTIAL FURTHER RESEARCH

5.1 STANDARDISED DIC MATERIAL TESTING METHODS

Based on the results of the testing carried out in this project, DIC appears to have great potential as a method for testing the shear modulus of timber, and likely other stiffness properties. For DIC to become common practice, standardised methods will need to be agreed upon such that results can be compared and correlated. Research will be needed to further demonstrate the potential of DIC, and to develop appropriate methods to ensure the results they produce are sufficiently reliable and reproduceable. It is thought that the alternative methods described here represent a good starting point.

5.2 STEEL COMPRESSION REINFORCEMENT ANALOGY FOR SCREWS

The phenomenon observed of relative displacement between screws in the region of overlap is clearly analogous to the behaviour of steel reinforcement lap lengths in reinforced concrete columns in compression. Some research has been done to investigate this analogy [7], but it is felt it would be a productive topic for further research.

6 CONCLUSIONS

In testing the properties of sweet chestnut, it became clear that material testing is a promising new application for Digital Image Correlation. It was able to implement methods based on the entire strain distributions rather than individual displacement readings, and with further refinement these methods could potentially be more robust and accurate than previous analogue methods. Methods could also be developed for obtaining material properties other than the shear modulus.

The testing and finite element modelling allowed the calculation of the overall stiffness of the roof, and highlighted challenges regarding the structure's buildability. It also led to a more in depth understanding of the load paths through the screws, revealing the phenomenon of relative displacement between adjacent screws due to axial force transfer through shear in the timber matrix.

A spring model was also built, and after optimisation is highly accurate and provided a more in depth understanding of the load paths through the timber. It can now be used as a design tool to predict the roof's compression behaviour, and also the forces induced by moisture movement - something which 3D-continuum finite element modelling could not achieve.

ACKNOWLEDGEMENTS

Martin Touhey, Lorna Roberts, David Layfield and Phil McLaren in CUED Structures Lab, Nigel Braden from In-wood Developments.

REFERENCES

[1] BSI, 2016. BS EN 338:2016, Structural timber – Strength classes

[2] BSI, 2010. BS EN 408:2010+A1:2012, Timber structures – Structural timber and glued laminated timber – Determination of some physical and mechanical properties

[3] McRobie, A.: AllanPIV, Matlab code for Digital Image Correlation, *University of Cambridge*

[4] Kaneko, T., On Timoshenko's correction for shear in vibrating beams. Journal of Physics D: Applied Physics, 8(16):1927. 1975

[5] Savitzky A., Golay M. J. E.: Smoothing and Differentiation of Data by Simplified Least Squares Procedures. Analytical Chemistry 36 (8):1627-1639, 1964.

[6] D'Assault Systemes, 2017. Abaqus

[7] Ramage, M., & Toumpanaki, E., 2018. Bond Performance of Glued-in CFRP and GFRP Rods in Timber. *INTER 2018: 5th Meeting of the International Network on Timber Engineering Research.* https://doi.org/10.17863/CAM.36481

[8] Tompkins, J.: Novel Timber Structures: Analysis of a Stacked Timber Roof.